Salomäki, J., Hinkkanen, M., and Luomi, J. (2008). Influence of inverter output filter on maximum torque and speed of PMSM drives. IEEE Transactions on Industry Applications, 44 (1), in press.

Influence of Inverter Output Filter on Maximum Torque and Speed of PMSM Drives

Janne Salomäki*, Marko Hinkkanen†, and Jorma Luomi†

*Konecranes Plc
P.O. Box 661, Koneenkatu 8
FI-05801 Hyvinkää, Finland
janne.salomaki@konecranes.com
†Power Electronics Laboratory
Helsinki University of Technology
P.O. Box 3000, FI-02015 TKK, Finland

***Abstract*— The paper deals with the maximum torque and speed of permanent magnet synchronous motor (PMSM) drives when the inverter output voltage is filtered by an LC filter with a cut-off frequency well below the switching frequency. According to steady-state analysis, the filter affects the performance of the motor drive especially at high speeds. The stator current is not equal to the inverter current, and due to the inverter current and inverter voltage limits, the torque-maximizing stator current locus differs from that of a drive without the filter. A field-weakening method is proposed for PMSM drives with an inverter output filter. The method is implemented and tested in a 2.2-kW PMSM drive. The experimental results agree well with the analysis, and validate the high-speed performance of the proposed field-weakening method.**

***Index Terms*— Permanent magnet synchronous motor (PMSM) drives, inverter output filter, field-weakening control, vector control.**

I. Introduction

Secondary effects of pulse-width modulation (PWM) are a concern in AC motors fed by modern voltage source inverters. The high rate of change of the inverter output voltage may cause excessive voltage stresses in the stator winding insulations of the motor [1]. The common-mode voltage and high-frequency leakage currents through the parasitic capacitances of the stator winding may lead to bearing currents and premature bearing failures [2]. Harmonics at the switching frequency and its multiples give rise to acoustic noise and extra losses in the motor. Although these problems have mainly been reported for induction motor drives, the concern is also relevant in permanent magnet synchronous motor (PMSM) drives [3]–[5]. A means to overcome the problems is using a sinusoidal inverter output filter, i.e. filtering the inverter output voltage with a three-phase LC filter with a cut-off frequency well below the switching frequency of the inverter. Recently proposed vector control methods make it possible to add an LC filter to the inverter output without adding any extra measurements to the AC drive [6]–[8]. The control performance is close to that of a drive without the filter.

Because of the limited inverter voltage, field weakening is used at high speeds. Various field-weakening control methods have been proposed for PMSM drives. The methods based on voltage control [9]–[11] provide full utilization of the dc-link voltage automatically. In [9], a PI-type voltage controller was used for interior PMSM drives to adjust the voltage reference up to the voltage capability of the inverter. The proposed control scheme enables only speed mode operation. A field-weakening method for surface-mounted PMSM drives [10] applied a similar voltage-control strategy with a modified input to the PI-controller. The field-weakening control was further developed in [11] for induction motor drives. The PI-type voltage controller was replaced with an I-controller to avoid an algebraic loop and to have only one control parameter for the field weakening.

In a drive equipped with an inverter output filter, the stator voltage and current differ from the corresponding inverter quantities. The maximum torque and speed are constrained by both the inverter current limit and the stator current limit in addition to the maximum voltage of the inverter. A field-weakening algorithm for induction motor drives equipped with an inverter output filter has been presented in [7], but the influence of the filter on the high-speed performance of PMSM drives has not yet been investigated.

In this paper, the theoretical maximum torque and speed of PMSM drives equipped with an inverter output filter are investigated by means of steady-state analysis. A field-weakening method based on voltage control is developed for these drives, enabling maximum-torque operation at high speeds. Laboratory experiments are used for investigating the proposed method.

II. Modelling of LC Filter and PMSM

Fig. 1 shows a PMSM drive equipped with an inverter output filter. The inverter output voltage $\mathbf{u}_A$ is filtered by

The paper was presented at the PCC Nagoya 2007 conference in April 2-5, 2007. This work was supported by ABB Oy, the Walter Ahlström Foundation, the Finnish Foundation of Technology, and the KAUTE Foundation.

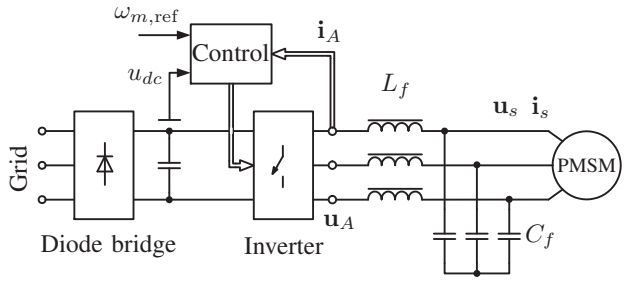

Fig. 1. PMSM drive equipped with three-phase LC filter.

the LC filter, resulting in a nearly sinusoidal stator voltage $\mathbf{u}_s$. The inverter output current $\mathbf{i}_A$ and the dc-link voltage u_{dc} are the only measured quantities.

In a reference frame rotating at angular frequency ω_m, the equations for the LC filter are

$$\frac{d\mathbf{i}_A}{dt} = -\frac{R_{Lf}}{L_f}\mathbf{i}_A - \omega_m \mathbf{J}\mathbf{i}_A + \frac{1}{L_f}(\mathbf{u}_A - \mathbf{u}_s) \quad (1)$$

$$\frac{d\mathbf{u}_s}{dt} = -\omega_m \mathbf{J}\mathbf{u}_s + \frac{1}{C_f}(\mathbf{i}_A - \mathbf{i}_s), \quad (2)$$

where $\mathbf{i}_A = \begin{bmatrix} i_{Ad} & i_{Aq} \end{bmatrix}^T$ is the inverter output current, $\mathbf{u}_A = \begin{bmatrix} u_{Ad} & u_{Aq} \end{bmatrix}^T$ the inverter output voltage, $\mathbf{u}_s = \begin{bmatrix} u_{sd} & u_{sq} \end{bmatrix}^T$ the stator voltage, $\mathbf{i}_s = \begin{bmatrix} i_{sd} & i_{sq} \end{bmatrix}^T$ the stator current, L_f the inductance and R_{Lf} the series resistance of the filter inductor, C_f the capacitance of the filter, and

$$\mathbf{J} = \begin{bmatrix} 0 & -1 \\ 1 & 0 \end{bmatrix}$$

In the *d-q* reference frame fixed to the rotor, the voltage equation of the PMSM is

$$\mathbf{u}_s = R_s \mathbf{i}_s + \frac{d\boldsymbol{\psi}_s}{dt} + \omega_m \mathbf{J}\boldsymbol{\psi}_s \quad (3)$$

where R_s is the stator resistance and ω_m the electrical angular speed of the rotor. The stator flux linkage is

$$\boldsymbol{\psi}_s = \mathbf{L}_s \mathbf{i}_s + \boldsymbol{\psi}_{pm} \quad (4)$$

where $\boldsymbol{\psi}_{pm} = \begin{bmatrix} \psi_{pm} & 0 \end{bmatrix}^T$ is the permanent magnet flux. The stator inductance matrix

$$\mathbf{L}_s = \begin{bmatrix} L_d & 0 \\ 0 & L_q \end{bmatrix}$$

consists of the direct-axis inductance L_d and quadrature-axis inductance L_q. The electromagnetic torque is

$$T_e = \frac{3p}{2}\boldsymbol{\psi}_s^T \mathbf{J}^T \mathbf{i}_s \quad (5)$$

where p is the number of pole pairs.

III. Steady-State Analysis

The maximum speed and torque of the PMSM depend on the voltage and current limits of the inverter and motor. In the following, the steady-state analysis of the PMSM [12] is extended to PMSM drives equipped with an inverter output filter. For simplicity, the filter resistance is ignored. This simplification does not cause significant errors since the inductive reactance of the filter inductor is much greater than the filter resistance at high speeds. The stator resistance is taken into account, unless otherwise stated. In the following examples, the data of a 2.2-kW interior PMSM drive are used. The system data are given in Table I. The base values of the angular frequency, current, and voltage are $2\pi \cdot 75$ rad/s, $\sqrt{2} \cdot 4.3$ A, and $\sqrt{2/3} \cdot 370$ V, respectively. The drive has a finite maximum speed since $i_{s,\max} < \psi_{pm}/L_d$. The operation of a drive with $i_{s,\max} \geq \psi_{pm}/L_d$ is briefly discussed at the end of this section.

TABLE I
Motor and Filter Data

Motor Ratings	
Power	2.2 kW
Voltage (phase-to-phase)	370 V, rms
Current	4.3 A, rms
Frequency	75 Hz
Speed	1500 r/min
Torque T_N	14.0 Nm
Motor Parameters	
Stator resistance R_s	3.59 Ω (0.072 p.u.)
Direct-axis inductance L_d	36.0 mH (0.34 p.u.)
Quadrature-axis inductance L_q	51.0 mH (0.48 p.u.)
Permanent magnet flux ψ_{pm}	0.545 Vs (0.88 p.u.)
Total moment of inertia J	0.015 kgm^2 (63.3 p.u.)
LC Filter Parameters	
Inductance L_f	5.1 mH (0.048 p.u.)
Capacitance C_f	6.8 μF (0.16 p.u.)
Series resistance R_{Lf}	0.1 Ω (0.002 p.u.)
Current and Voltage Limits	
Inverter current $i_{A,\max}$	9.1 A (1.5 p.u.)
Stator current $i_{s,\max}$	9.1 A (1.5 p.u.)
Inverter voltage $u_{A,\max}$ (phase-to-neutral)	$540/\sqrt{3}$ V (1.03 p.u.)

A. Current Limits

The inverter output current and the stator current differ from each other when an LC filter is used. Therefore, the maximum inverter current $i_{A,\max}$ and the maximum stator current $i_{s,\max}$ are defined separately. The stator current components i_{sd} and i_{sq} are limited according to

$$i_{sd}^2 + i_{sq}^2 \leq i_{s,\max}^2 \quad (6)$$

The feasible stator current has a circular boundary in the i_{sd}-i_{sq} plane as shown in Fig. 2 (dashed line).

Similarly, the inverter current components i_{Ad} and i_{Aq} are limited according to

$$i_{Ad}^2 + i_{Aq}^2 \leq i_{A,\max}^2 \quad (7)$$

The steady-state solution of (2)–(4) yields the inverter current as a function of the stator current:

$$i_{Ad} = (1 - \omega_m^2 C_f L_d) i_{sd} - \omega_m C_f R_s i_{sq} - \omega_m^2 C_f \psi_{pm} \quad (8)$$

$$i_{Aq} = \omega_m C_f R_s i_{sd} + (1 - \omega_m^2 C_f L_q) i_{sq} \quad (9)$$

According to (7)–(9), the inverter current limit corresponds to a speed-dependent elliptical boundary for the feasible

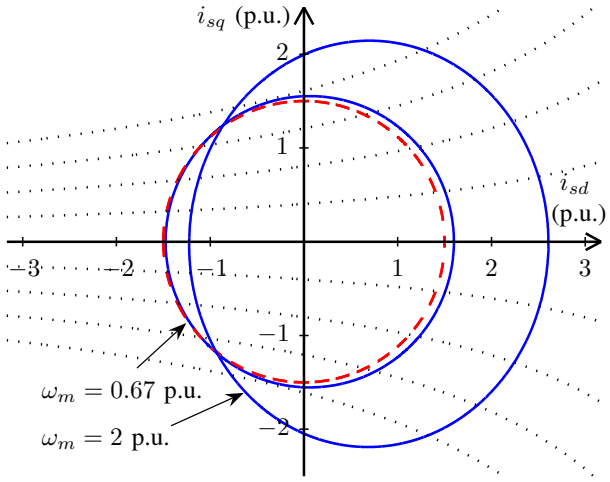

Fig. 2. Inverter current limit at two speeds (solid) and stator current limit (dashed) in i_{sd}-i_{sq} plane for $i_{A,\max} = i_{s,\max} = 1.5$ p.u. Constant-torque curves (dotted) are also shown.

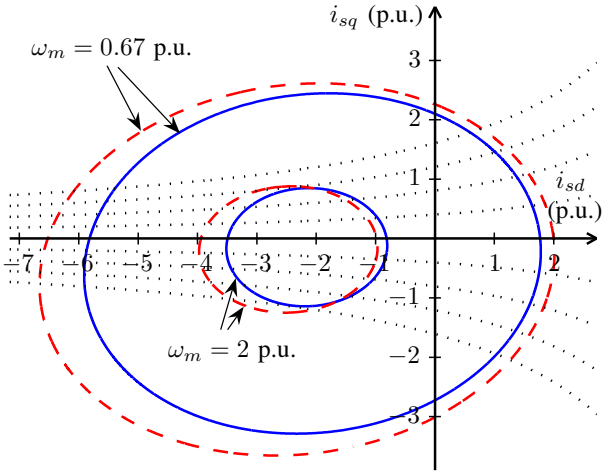

Fig. 3. Inverter voltage limits in i_{sd}-i_{sq} plane for rotor speed values of 0.67 p.u. and 2 p.u. Solid lines are for a drive with an LC filter and dashed lines for a drive without a filter. Constant-torque curves (dotted) are also shown.

stator current in the i_{sd}-i_{sq} plane as shown in Fig. 2 (solid lines). In this analysis, the inverter and stator current limits are equal. Consequently, the inverter current limit ellipse approaches the circle defined by the stator current limit at low speeds.

B. Voltage Limit

The dc-link voltage constrains the inverter output voltage. Omitting the possible overmodulation, the maximum inverter output voltage is $u_{A,\max} = u_{dc}/\sqrt{3}$, and the inverter voltage components u_{Ad} and u_{Aq} are limited according to

$$u_{Ad}^2 + u_{Aq}^2 \leq u_{A,\max}^2 \tag{10}$$

The steady-state solution of (1)–(4) gives the inverter voltage as a function of the stator current:

$$\begin{aligned} u_{Ad} &= (1 - \omega_m^2 L_f C_f) R_s i_{sd} \\ &\quad + (\omega_m^2 L_f C_f L_q - L_f - L_q)\omega_m i_{sq} \qquad (11) \\ u_{Aq} &= (-\omega_m^2 L_f C_f L_d + L_f + L_d)\omega_m i_{sd} \\ &\quad + (1 - \omega_m^2 L_f C_f) R_s i_{sq} \\ &\quad + (1 - \omega_m^2 L_f C_f)\omega_m \psi_{pm} \qquad (12) \end{aligned}$$

Substituting (11) and (12) for the inverter voltage components in (10) yields a speed-dependent elliptical boundary for the feasible stator current in the i_{sd}-i_{sq} plane as shown in Fig. 3 (solid lines). If the filter is not present, the ellipses are changed as illustrated in Fig. 3 (dashed lines).

C. Theoretical Maximum Torque

The theoretical maximum torque can be determined in steady state as a function of the rotor speed from the torque expression (5) constrained by (6)–(12). Fig. 4 shows an example stator current locus for the maximum torque operation as the steady-state speed is varied.

At low speeds, the maximum torque is obtained at the intersection of the maximum torque-per-ampere (MTPA) trajectory and the stator current limit circle (point A).

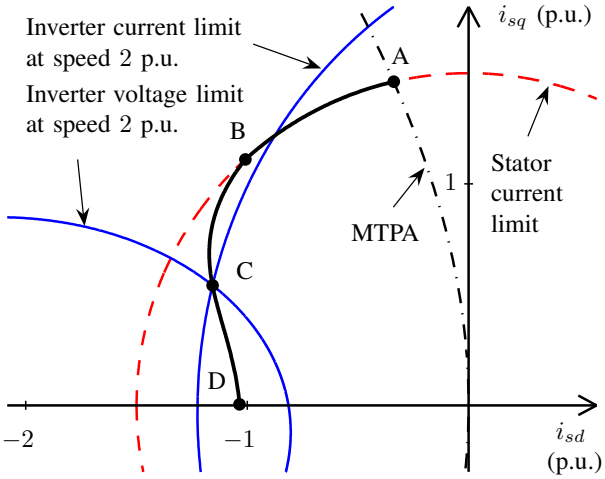

Fig. 4. Torque-maximizing stator current locus as steady-state speed is varied. The inverter current and voltage limits are shown for a speed of 2 p.u., corresponding to operating point C.

This operation point is possible up to the speed at which the voltage limit ellipse intersects the stator current limit circle at point A. As the speed increases further and, consequently, the voltage limit ellipse shrinks, the torque-maximizing stator current locus moves along the stator current limit circle (A→B). Both the stator current and inverter voltage limits are active, and the drive operates in the field-weakening region.

Without the LC filter, the torque-maximizing stator current locus proceeds along the stator current limit circle. When the LC filter is present, the inverter current limit becomes active instead of the stator current limit at a speed of 1.3 p.u. corresponding to point B. At higher speeds, the torque-maximizing stator current stays at the intersection of the inverter current and voltage limit curves, but this intersection moves as the limit curves change with the speed (B→D). In Fig. 4, the inverter current and voltage limit curves are plotted only for a single speed of 2 p.u. corresponding to operating point C. Fig. 5 shows space

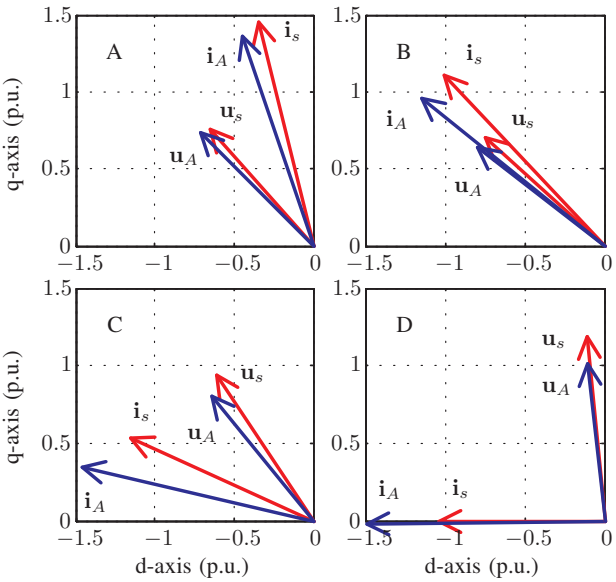

Fig. 5. Space vector diagrams corresponding to the operating points A, B, C, and D in Fig. 4. The rotor speed is A: $\omega_m = 0.9$ p.u.; B: $\omega_m = 1.3$ p.u.; C: $\omega_m = 2$ p.u., and D: $\omega_m = 2.4$ p.u.

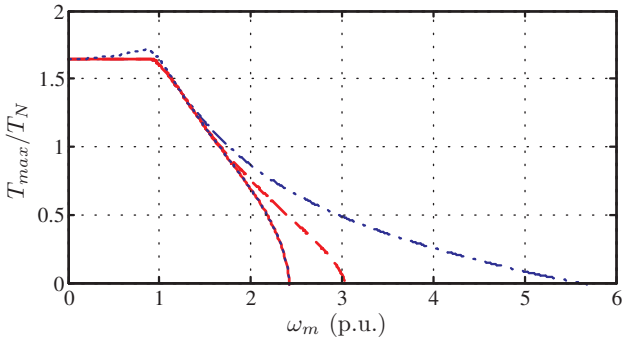

Fig. 6. Maximum torque as function of rotor speed. Solid line is for drive with LC filter and $i_{A,\max} = i_{s,\max} = 1.5$ p.u., dashed line for drive without filter, dotted line is for drive with LC filter and $i_{A,\max} = 1.5$ p.u. (no limit for $i_{s,\max}$, coincides the solid line at high speeds), and dash dotted line is for drive with LC filter and $i_{s,\max} = 1.5$ p.u. (no limit for $i_{A,\max}$).

vector diagrams corresponding to the operating points A, B, C, and D.

The influence of the LC filter on the maximum torque and the maximum speed is illustrated in Fig. 6. All curves are based on the same inverter voltage limit ($u_{A,\max} = 540/\sqrt{3}$ V). If the inverter and stator current limits are equal (solid line), the drive with the LC filter produces nearly the same maximum torque as the drive without the filter (dashed line) up to almost twice the nominal speed in the example drive. Above that speed, the LC filter reduces the maximum torque, and the maximum speed is also reduced. If only the inverter current is limited (dotted line), the maximum torque around the nominal speed is higher with the LC filter than without it. On the other hand, the LC filter increases the maximum speed and the maximum torque at high speeds if only the stator current is limited (dash dotted line). The magnitude of the inverter current is $|\mathbf{i}_A| = 2.0$ p.u. at the speed $\omega_m = 3$ p.u. and $|\mathbf{i}_A| = 2.8$ p.u. at the speed $\omega_m = 5$ p.u.

D. Theoretical Maximum Speed

The motor can operate only inside the current and voltage limit ellipses. The theoretical maximum speed for given voltage and current limits is obtained when the overlapping region has shrunk to a single point, i.e. the voltage limit ellipse touches the current limit ellipse (or circle). In the following maximum speed analysis, the filter resistance and the stator resistance are ignored.

At the maximum speed, the torque-producing current component i_{sq} equals zero. Without the filter, the maximum speed is [13]

$$\omega_{m,\max} = \frac{u_{s,\max}}{\psi_{pm} - L_d i_{s,\max}} \tag{13}$$

It is to be noted that if $i_{s,\max} \geq \psi_{pm}/L_d$, the voltage limit ellipse shrinks inside the circle defined by the stator current limit as the speed increases, and the theoretical maximum speed is infinite.

When the LC filter is present, the maximum speed depends on which one of the current limits is active. Eqs. (14) and (15) below correspond to the inverter current limit $i_{A,\max}$ and the stator current limit $i_{s,\max}$, respectively. The maximum speed is obtained by solving ω_m from each of these equations and selecting the lower value.

The solutions of (13), (14), and (15) for the example drive are 3.05 p.u., 2.43 p.u., and 5.82 p.u., respectively. Thus, the LC filter reduces the maximum speed if $i_{A,\max} \leq i_{s,\max}$. On the other hand, if $i_{A,\max}$ is much greater than $i_{s,\max}$, the maximum speed is higher with the filter than without it.

E. Example of Infinite-Maximum-Speed Drive

In order to analyze the theoretical maximum torque of an infinite-maximum-speed PMSM drive (i.e. $i_{s,\max} \geq \psi_{pm}/L_d$), the system data was kept unchanged with the exception of $\psi_{pm} = 0.2725$ Vs (0.44 p.u.). This permanent magnet flux value is used only in the following analysis.

Fig. 7 shows the stator current locus for the maximum torque operation. The inverter current limit and the inverter voltage limit are plotted at speeds 3.33 p.u. and 7 p.u. A maximum torque per inverter voltage (MTPIV) curve is obtained by maximizing the torque (5) with the constraints

$$L_d L_f C_f i_{A,\max} \omega_m^3 + L_d C_f u_{A,\max} \omega_m^2 + (\psi_{pm} - L_f i_{A,\max} - L_d i_{A,\max})\omega_m - u_{A,\max} = 0 \tag{14}$$

$$(L_d L_f C_f i_{s,\max} - L_f C_f \psi_{pm})\omega_m^3 + (\psi_{pm} - L_f i_{s,\max} - L_d i_{s,\max})\omega_m - u_{A,\max} = 0 \tag{15}$$

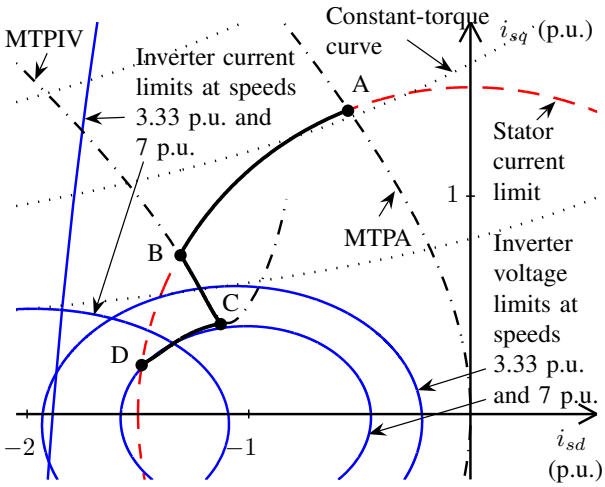

Fig. 7. Torque-maximizing stator current locus of infinite-maximum-speed PMSM drive as steady-state speed is varied. The inverter current and voltage limits are shown for speeds 3.33 p.u. and 7 p.u.

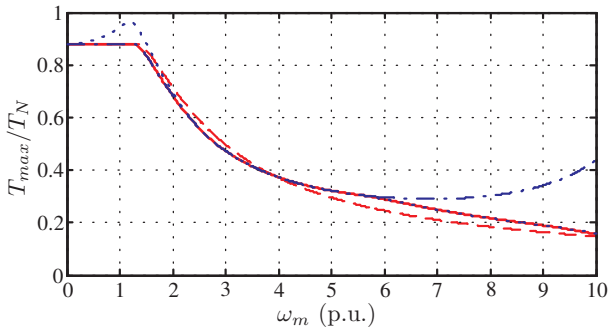

Fig. 8. Maximum torque of infinite-maximum-speed PMSM drive as function of rotor speed. Explanations of the curves are as in Fig 6.

(10)–(12) at different speeds. As the speed increases after point B, the maximum torque is obtained at the intersection of the MTPIV curve and the voltage limit curve (B→C). The inverter voltage limit is the only active limit between points B and C. The shape of the inverter current limit curve changes significantly at the speed $\omega_m = \sqrt{1/(C_f L_d)}$, which is the parallel resonance frequency of the filter capacitor and the stator inductance. The inverter current limit becomes active at a speed corresponding to operating point C. The torque-maximizing stator current stays at the intersection of the inverter current and voltage limit curves, but this intersection moves as the limit curves change with the speed (C→D). Finally, the stator current limit circle is reached at point D. The stator current locus is plotted up to a speed of 10 p.u., which is close to the filter resonance frequency. Above that speed, the analysis is no longer reasonable.

Fig. 8 shows the maximum torque as a function of rotor speed. If only the inverter current is limited (dotted line), the maximum torque around the nominal speed is higher with the LC filter than without it. Otherwise, the LC filter does not affect the maximum torque of the drive significantly. It is to be noted that if only the stator current is limited (dash dotted line), the inverter current gets unreasonably high values at speeds above 6 p.u.

IV. Torque-Maximizing Field-Weakening Control

As was shown in the previous section, the LC filter affects the torque capability of the PMSM drive. Consequently, the field-weakening control should be modified for PMSM drives equipped with the LC filter in order to achieve maximum torque operation and good dynamic performance at high speeds. In the following, a field-weakening method based on voltage control similar to [11] is developed for these drives. The inverter current limitation is added, and the LC filter is taken into account in the determination of the voltage controller gain.

A. Field-Weakening Control Algorithm

The block diagram of the proposed field-weakening control is shown in Fig. 9. The field weakening is implemented by adding an incremental d-axis stator current reference $i_{sd\Delta}$ to the d-axis current reference $i_{sd\mathrm{M}}$ that is in accordance with the MTPA trajectory. The d-axis current reference is thus

$$i_{sd,\mathrm{ref}} = i_{sd\mathrm{M}} + i_{sd\Delta} \tag{16}$$

The voltage control algorithm is

$$\frac{di_{sd\Delta}}{dt} = \gamma_f \left[u_{A,\max}^2 - (u'_{A,\mathrm{ref}})^2\right], \quad i_{sd\Delta,\min} \le i_{sd\Delta} \le 0 \tag{17}$$

where γ_f is the controller gain and $u'_{A,\mathrm{ref}}$ is the magnitude of the unlimited inverter voltage reference. The lower limit of $i_{sd\Delta}$ is designed as

$$i_{sd\Delta,\min} = -i_{sd\mathrm{M}} + \max\left\{-i_{s,\max}, \frac{i_{A,\max} - \hat{\omega}_m^2 C_f \psi_{pm}}{\hat{\omega}_m^2 C_f L_d - 1}\right\} \tag{18}$$

The second term inside the maximum function is based on (8) assuming $R_s = 0$, preventing the violation of the inverter current limit.

The q-axis stator current reference is limited according to

$$i_{sq,\mathrm{ref}} = \mathrm{sign}(i'_{sq,\mathrm{ref}}) \cdot \min\left\{|i'_{sq,\mathrm{ref}}|, \sqrt{i_{s,\max}^2 - i_{sd,\mathrm{ref}}^2}, \frac{\sqrt{i_{A,\max}^2 - \left[(\hat{\omega}_m^2 C_f L_d - 1) i_{sd,\mathrm{ref}} + \hat{\omega}_m^2 C_f \psi_{pm}\right]^2}}{1 - \hat{\omega}_m^2 L_q C_f}\right\} \tag{19}$$

The minimum of the three values is chosen: (i) the absolute value of the unlimited reference $i'_{sq,\mathrm{ref}}$; (ii) the value defined by the stator current limit according to (6); or (iii) the value defined by the inverter current limit according to (7)–(9) assuming $R_s = 0$.

It is to be noted that the algorithm does not take into account drives in which the center point of the voltage limit ellipse is located inside the stator current limit circle. These so called infinite-maximum-speed PMSM drives require special control techniques at very high speeds [14]–[16].

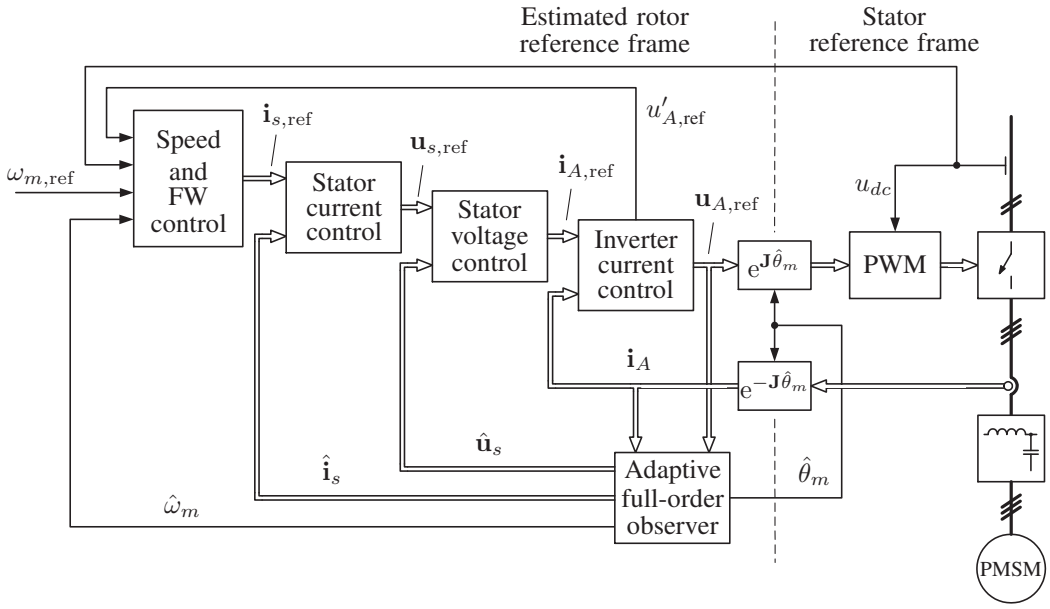

Fig. 10. Simplified block diagram of the control system. Double lines indicate vector quantities whereas single lines indicate scalar quantities. The speed and field-weakening (FW) control is shown in detail in Fig. 9.

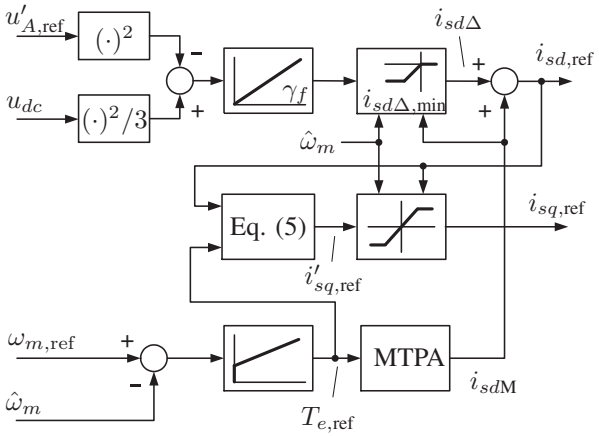

Fig. 9. Speed control and field-weakening control.

B. Gain Selection

Desired closed-loop dynamics of the flux-producing current component i_{sd} are obtained in the field weakening by selecting the gain γ_f. When (12) is approximated by

$$u_{Aq} = (L_f + L_d)\omega_m i_{sd} + \omega_m \psi_{pm}$$

and by assuming that $i_{sd,\mathrm{ref}} = i_{sd}$, $R_s = 0$, $u_{Ad0} = 0$, $u_{Aq0} = u_{A,\max}\mathrm{sign}\{\omega_{m0}\}$, the linearization of (16)–(17) results in

$$\frac{d\tilde{i}_{sd}}{dt} \approx -2\gamma_{f0} u_{A,\max} |\omega_{m0}| (L_f + L_d)\tilde{i}_{sd} \qquad (20)$$

The operating-point quantities are denoted by subscript 0, and deviations about the operating point are marked by a tilde.

The gain γ_f can be determined by selecting the bandwidth α_f of (20). The result is

$$\gamma_f = \frac{\alpha_f}{2u_{A,\max}\omega'_m(L_f + L_d)} \qquad (21)$$

Too high gain values are avoided at low speeds by selecting ω'_m as

$$\omega'_m = \begin{cases} \omega_\gamma, & \text{if } |\hat{\omega}_m| \le \omega_\gamma \\ |\hat{\omega}_m|, & \text{otherwise} \end{cases} \qquad (22)$$

where ω_γ is an approximate angular speed limit for the field weakening.

V. Speed-Sensorless Vector Control

The control of the PMSM drive equipped with an inverter output filter is based on cascaded controllers and a speed-adaptive full-order observer as presented in [8]. Fig. 10 shows a simplified block diagram of the control system (the estimated quantities being marked by ˆ). The cascade control and the speed-adaptive full-order observer are implemented in the estimated rotor reference frame. The estimated rotor position $\hat{\theta}_m$ is obtained by integrating $\hat{\omega}_m$. The inverter current is the feedback signal for the observer. The observer gain is chosen as in [8] resulting in a locally stable observer in a wide speed range. In practice, however, the inverter non-idealities and the inaccuracies of the system parameters cause stability problems in sustained operation at low speeds under load. These problems can be solved by augmenting the adaptive observer with a signal injection method [17]. Signal injection is not used in the following experimental results.

The inverter current, the stator voltage, and the stator current are controlled by PI controllers, and cross-couplings due to the rotating reference frame are compensated. A simple one-step-ahead current prediction is

used in the inverter current control in a fashion similar to [18]. The rotor speed control and field-weakening control are based on Fig. 9. Active damping and integrator anti-windup are included in the speed control (not shown in the block diagram). The stator current reference is in accordance with the MTPA at low speeds. The use of the torque expression (5) after the computation of the d-axis stator current reference enables torque-mode operation.

In the following experimental results, the bandwidths of the controllers are $2\pi \cdot 600$ rad/s for the inverter current, $2\pi \cdot 400$ rad/s for the stator voltage, $2\pi \cdot 200$ rad/s for the stator current, and $2\pi \cdot 4$ rad/s for the rotor speed. The parameters for the field-weakening control are $\alpha_f = 2\pi \cdot 20$ rad/s and $\omega_\gamma = 2\pi \cdot 50$ rad/s. A voltage margin of 4 % is added to improve the performance in transient states.

VI. Experimental Results

The experimental setup consists of a frequency converter controlled by a dSPACE DS1103 PPC/DSP board, a 2.2-kW six-pole interior PMSM, and a three-phase LC filter. The motor and filter data are given in Table I. Mechanical load is provided by a servo drive. The sampling frequency is equal to the switching frequency of 5 kHz.

Fig. 11 shows an acceleration from zero speed to 2 p.u. at no load when $i_{A,\max} = i_{s,\max} = 1.5$ p.u. Before the acceleration, the speed-adaptive observer is stable at zero speed because there is no load. The drive operates the first 0.12 s after the speed reference step at constant torque until the inverter voltage limit is reached. Then, the field-weakening control rapidly reduces the d-axis stator current. The rotor speed reaches its reference value in approximately 0.4 s.

Fig. 12 shows the voltage and current waveforms at the operating point corresponding to the final state in Fig. 11. The inverter output current exceeds the limit $i_{A,\max} = 1.5$ p.u. momentarily because the control does not take into account the switching oscillation. The stator voltage and the stator current are nearly sinusoidal.

Fig. 13 shows experimental results as the PMSM drive with the LC filter was in the torque mode. The torque reference was set well above the maximum torque at $t = 0.5$ s. The speed was controlled by the servo drive from 0.4 p.u. to 2 p.u. in 20 seconds. The drive operates the first 6.5 s after the torque reference step at constant torque corresponding to point A in Fig. 4. At low speeds, the inverter and stator currents are close to each other. As the speed increases, the current difference increases as was expected according to the steady-state analysis. Fig. 14 shows the trajectory of the estimated stator current. The trajectory is close to the steady-state stator current locus shown in Fig. 4. The drawn inverter current and voltage limit ellipses correspond to those in Fig. 4 with the exception that $u_{A,\max} \approx 0.96 \cdot 545/\sqrt{3}$ V.

Fig. 15 shows experimental results as the PMSM drive with the LC filter was in the torque mode, and the servo drive maintained a constant speed of 1.33 p.u. The torque reference of the PMSM with the LC filter was slowly raised from zero to $1.3T_N$. The figure shows the trajectory of the estimated stator current. The inverter current and voltage limits are drawn for $\omega_m = 1.33$ p.u. The stator current proceeds along the inverter voltage limit ellipse. At low torque, the d-axis stator current differs from the voltage limit ellipse because the dc-link voltage is higher at no load than under load.

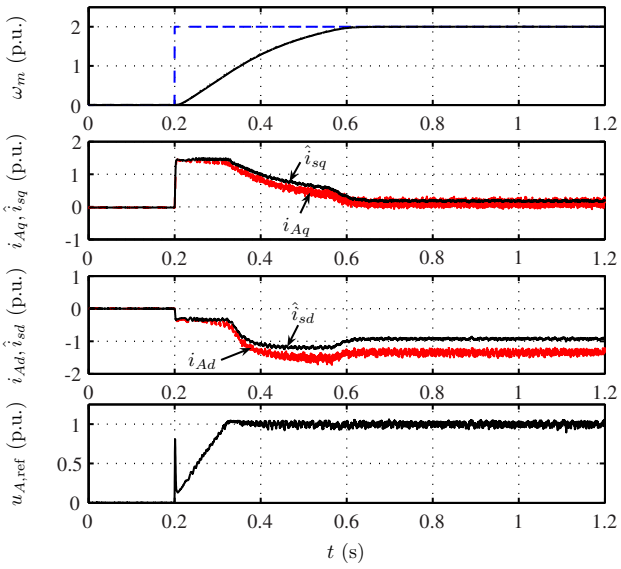

Fig. 11. Experimental results showing acceleration from zero speed to 2 p.u. The first subplot shows the speed reference (dashed), the actual rotor speed (solid), and its estimate (dotted, coincides the solid line). The second subplot shows the q components of the estimated stator current and actual inverter current. The third subplot shows the d components of the estimated stator current and actual inverter current. The fourth subplot shows the magnitude of the inverter voltage reference.

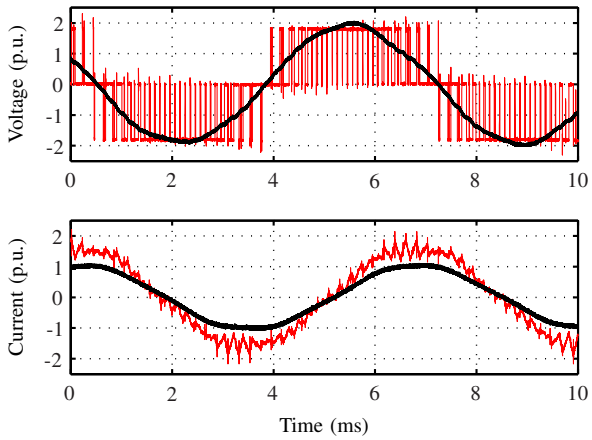

Fig. 12. Measured voltage and current waveforms at $\omega_m = 2$ p.u. without load. The first subplot shows the inverter output voltage (phase to phase) and the stator voltage (phase to phase). The second subplot shows the inverter output current and the stator current.

VII. Conclusion

The steady-state analysis shows that an inverter output LC filter affects the maximum torque and speed of a finite-maximum-speed PMSM drive significantly. If the inverter and stator current limits are equal, the maximum torque is lowered at the highest speeds in the field-weakening region

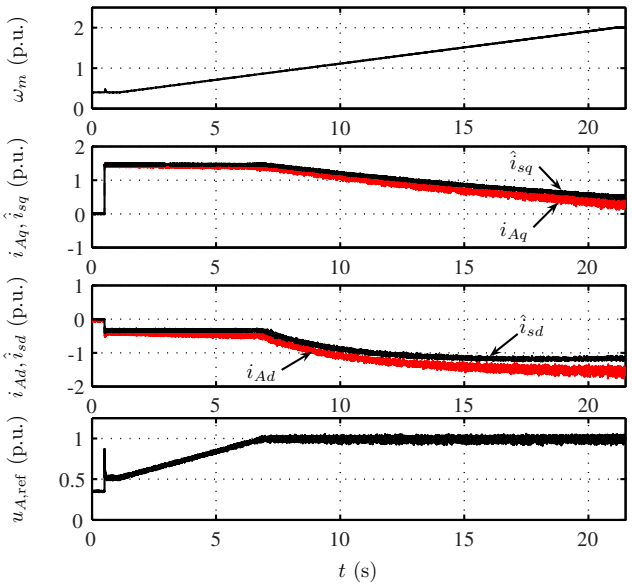

Fig. 13. Experimental results showing torque-mode operation as the speed is slowly increased and PMSM drive with LC filter provides as much torque as possible. The explanations of the curves as in Fig. 11.

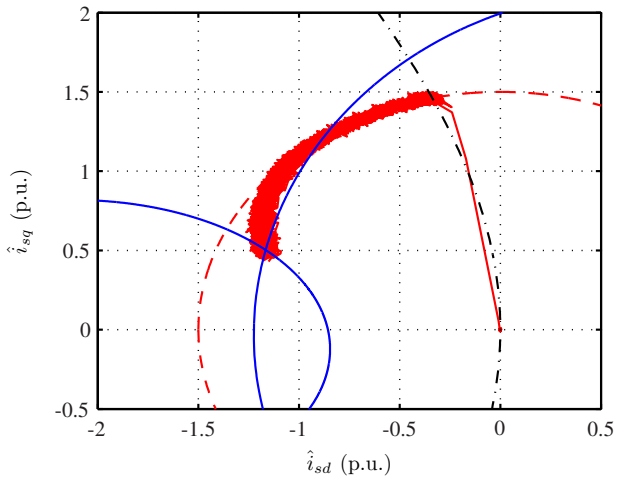

Fig. 14. Experimental results showing estimated stator current trajectory from experiment in Fig. 13. The voltage limit ellipse is drawn using $u_{A,\max} = 0.96 \cdot 545/\sqrt{3}$ V.

as compared to a drive without the filter, and the maximum speed is decreased. If the stator current is allowed to be higher than the inverter current limit, the maximum torque increases around the nominal speed. If the inverter current limit is clearly higher than the stator current limit, both the maximum torque in the field-weakening region and the maximum speed can be higher than those of a drive without the filter. In a infinite-maximum-speed PMSM drive, the LC filter does not affect the maximum torque at high speeds significantly. The proposed field-weakening control algorithm for finite-maximum-speed PMSM drives equipped with an LC filter enables the maximum-torque operation at high speeds. The experimental results agree well with the steady-state analysis, and validate the performance of the field-weakening method.

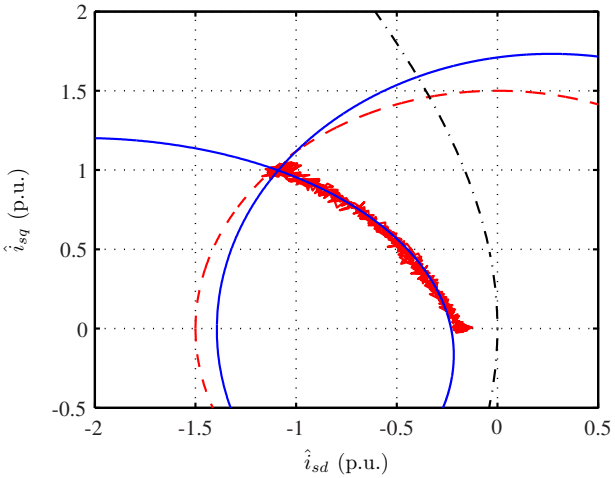

Fig. 15. Experimental results showing estimated stator current trajectory as torque reference is slowly raised and rotor speed is constant $\omega_m = 1.33$ p.u. The voltage limit ellipse is drawn using $u_{A,\max} = 0.96 \cdot 545/\sqrt{3}$ V.

ACKNOWLEDGMENT

The authors would like to thank the reviewers for their insightful comments and suggestions. The technical help with the experimental setup provided by Mr. Antti Piippo and Mr. Markus Oinonen is also gratefully acknowledged.

REFERENCES

[1] E. Persson, "Transient effects in application of PWM inverters to induction motors," *IEEE Trans. Ind. Applicat.*, vol. 28, no. 5, pp. 1095–1101, Sept./Oct. 1992.

[2] S. Chen, T. A. Lipo, and D. Fitzgerald, "Source of induction motor bearing currents caused by PWM inverters," *IEEE Trans. Energy Conversion*, vol. 11, no. 1, pp. 25–32, Mar. 1996.

[3] M. Carpita, D. Colombo, A. Monti, and A. Fradilli, "Power converter filtering techniques design for very high speed drive systems," in *Proc. EPE'01*, Graz, Austria, Aug. 2001.

[4] T. D. Batzel and K. Y. Lee, "Electric propulsion with sensorless permanent magnet synchronous motor: implementation and performance," *IEEE Trans. Energy Conversion*, vol. 20, no. 3, pp. 575–583, Sep. 2005.

[5] K. Yamazaki and Y. Seto, "Iron loss analysis of interior permanent-magnet synchronous motors-variation of main loss factors due to driving condition," *IEEE Trans. Ind. Applicat.*, vol. 42, no. 4, pp. 1045–1052, July/Aug. 2006.

[6] J. Salomäki and J. Luomi, "Vector control of an induction motor fed by a PWM inverter with output LC filter," *EPE Journal*, vol. 16, no. 1, pp. 37–43, Jan.-Mar. 2006.

[7] J. Salomäki, M. Hinkkanen, and J. Luomi, "Sensorless control of induction motor drives equipped with inverter output filter," *IEEE Trans. Ind. Electron.*, vol. 53, no. 4, pp. 1188–1197, Aug. 2006.

[8] J. Salomäki, A. Piippo, M. Hinkkanen, and J. Luomi, "Sensorless vector control of PMSM drives equipped with inverter output filter," in *Proc. IEEE IECON'06*, Paris, France, Nov. 2006, pp. 1059–1064.

[9] J.-M. Kim and S.-K. Sul, "Speed control of interior permanent magnet synchronous motor drive for the flux weakening operation," *IEEE Trans. Ind. Applicat.*, vol. 33, no. 1, pp. 43–48, Jan./Feb. 1997.

[10] D. S. Maric, S. Hiti, C. C. Stancu, and J. M. Nagashima, "Two improved flux weakening schemes for surface mounted permanent magnet synchronous machine drives employing space vector modulation," in *Proc. IEEE IECON'98*, vol. 1, Aachen, Germany, Aug./Sept. 1998, pp. 508–512.

[11] L. Harnefors, K. Pietiläinen, and L. Gertmar, "Torque-maximizing field-weakening control: design, analysis, and parameter selection," *IEEE Trans. Ind. Electron.*, vol. 48, no. 1, pp. 161–168, Feb. 2001.

[12] W. L. Soong and T. J. E. Miller, "Theoretical limitations to the field-weakening performance of the five classes of brushless synchronous AC motor drive," in *Electrical Machines and Drives Conf.*, Oxford, U.K., Sep. 1993, pp. 127–132.
[13] T. Sebastian and G. R. Slemon, "Operating limits of inverter-driven permanent magnet motor drives," *IEEE Trans. Ind. Applicat.*, vol. 23, no. 2, pp. 327–333, Mar./Apr. 1987.
[14] S. Morimoto, Y. Takeda, T. Hirasa, and K. Taniguchi, "Expansion of operating limits for permanent magnet motor by current vector control considering inverter capacity," *IEEE Trans. Ind. Applicat.*, vol. 26, no. 5, pp. 866–871, Sep./Oct. 1990.
[15] B.-H. Bae, N. Patel, S. Schulz, and S.-K. Sul, "New field weakening technique for high saliency interior permanent magnet motor," in *Conf. Rec. IEEE-IAS Annu. Meeting*, vol. 2, Salt Lake City, UT, Oct. 2003, pp. 898–905.
[16] G. Gallegos-Lopez, F. S. Gunawan, and J. E. Walters, "Optimum torque control of permanent-magnet AC machines in the field-weakened region," *IEEE Trans. Ind. Applicat.*, vol. 41, no. 4, pp. 1020–1028, July/Aug 2005.
[17] A. Piippo, J. Salomäki, and J. Luomi, "Signal injection in sensorless PMSM drives equipped with inverter output filter," in *Proc. PCC Nagoya 2007*, Nagoya, Japan, Apr. 2007, pp. 1105–1110.
[18] L. Springob and J. Holtz, "High-bandwidth current control for torque-ripple compensation in PM synchronous machines," *IEEE Trans. Ind. Electron.*, vol. 45, no. 5, pp. 713–721, Oct. 1998.

Janne Salomäki (GSM'06) is currently an R&D Engineer at Konecranes in Finland. From 2003 to 2007, he was a Researcher at the Power Electronics Laboratory, Helsinki University of Technology. His main research interest is the control of electric drives. He received his M.Sc.(Eng.) degree from Helsinki University of Technology, Espoo, Finland, in 2003. If all goes as planned, he will defend his PhD dissertation before this article is published.

Marko Hinkkanen (M'06) is currently an Acting Professor in the Department of Electrical and Communications Engineering, Helsinki University of Technology, Espoo, Finland. Since 2000, he has been with the Power Electronics Laboratory, Helsinki University of Technology. His research interests are in the areas of electric drives and electric machines. He received the M.Sc.(Eng.) and D.Sc.(Tech.) degrees from Helsinki University of Technology, in 2000 and 2004, respectively.

Jorma Luomi (M'92) is a Professor in the Department of Electrical and Communications Engineering, Helsinki University of Technology, Espoo, Finland. He joined Helsinki University of Technology in 1980, and from 1991 to 1998 he was a Professor at Chalmers University of Technology. His research interests are in the areas of electric drives, electric machines, and numerical analysis of electromagnetic fields. He received the M.Sc.(Eng.) and D.Sc.(Tech.) degrees from Helsinki University of Technology, in 1977 and 1984, respectively.